TISSUE ENGINEERING: Part A
Volume 20, Numbers 21 and 22, 2014

DOI: 10.1089/ten.tea.2014.0060

Engineered Skeletal Muscle Units for Repair of Volumetric Muscle Loss in the Tibialis Anterior Muscle of a Rat

Keith W. VanDusen, MS,[1] Brian C. Syverud, MS,[2] Michael L. Williams, BS,[1]
Jonah D. Lee, PhD,[1] and Lisa M. Larkin, PhD[1,2]

Volumetric muscle loss (VML) is the traumatic, degenerative, or surgical loss of muscle tissue, which may result in function loss and physical deformity. To date, clinical treatments for VML—the reflected muscle flap or transferred muscle graft—are limited by tissue availability and donor site morbidity. To address the need for more innovative skeletal muscle repair options, our laboratory has developed scaffoldless tissue-engineered skeletal muscle units (SMUs), multiphasic tissue constructs composed of engineered skeletal muscle with engineered bone-tendon ends, myotendinous junctions, and entheses, which *in vitro* can produce force both spontaneously and in response to electrical stimulation. Though phenotypically immature *in vitro*, we have shown that following 1 week of implantation in an ectopic site, our muscle constructs develop vascularization and innervation, an epimysium-like outer layer of connective tissue, an increase in myosin protein content, formation of myofibers, and increased force production. These findings suggest that our engineered muscle tissue survives implantation and develops the interfaces necessary to advance the phenotype toward adult muscle. The purpose of this study was to evaluate the potential of our SMUs to restore muscle tissue to sites of acute VML. Our results indicate that our SMUs continue to mature *in vivo* with longer recovery times and have the potential to repair VML sites by providing additional muscle fibers to damaged muscles. We conclude from this study that our SMUs have the potential to restore lost tissue volume in cases of acute VML.

Introduction

Multiple pathological conditions, including traumatic injuries, congenital defects, postoperative damage, and degenerative myopathies, can lead to volumetric loss of skeletal muscle tissue. Volumetric muscle loss (VML) is the loss of muscle tissue that exceeds the body's capacity for self-repair, resulting in impaired muscle function, and in many cases, physical deformity.[1,2] While many musculoskeletal traumas may be endogenously repaired over time through the myogenic potential of satellite cells, more severe cases of VML overwhelm this native repair mechanism, creating a need for surgical intervention.[3] The diversity of VML cases along with the functional and metabolic demands of muscle tissue complicates surgical repair, so while several repair strategies exist, all have significant limitations.[1] The primary treatment strategies involve muscle flap transposition or autologous tissue transfer.[4–9] Although each procedure type has demonstrated some success, both are limited by donor site morbidity and lack of available graft tissue. Thus, a demand exists for exogenous graft muscle tissue, prompting tissue engineering approaches to be increasingly investigated as potential strategies for VML treatment.

Since Vandenburgh's first work in 1988 suspending myotubes in a collagen gel and Dennis's first work in 2000 generating scaffoldless three-dimensional (3D) constructs that produced a physiological response similar to native muscle,[10–12] there continues to be significant research done in the area of skeletal muscle tissue engineering. While no laboratory has successfully yet engineered muscle that is functionally or phenotypically equivalent to adult skeletal muscle,[13–17] our group has developed a reproducible technique for engineering scaffold-free 3D skeletal muscle tissue constructs with functional myotendinous and neuromuscular interfaces, and has recently initiated implantation studies.[18,19–23] These skeletal muscle units (SMUs) contract spontaneously, producing $\sim 50\,\mu N$ of force *in vitro*, and when stimulated electrically, they produce an average maximum isometric force of $192 \pm 41\,\mu N$ *in vitro*.[18] Previously, we have shown that following only 1 week of implantation in an ectopic site, the maximum isometric force increased 286% to an average of $549 \pm 103\,\mu N$.[18] When their maximal tetanic forces are normalized to cross-sectional area (CSA), the engineered muscle produces a specific force of $1945\,N/m^2$, one of the highest recorded specific forces generated by an engineered 3D skeletal muscle. We hypothesize that implanting

Departments of [1]Molecular and Integrated Physiology and [2]Biomedical Engineering, University of Michigan, Ann Arbor, Michigan.

our SMUs for greater periods of time will further increase their contractile strength.

For restoration of function following VML injury, several interfaces must be established between host and graft tissues. For optimal force transmission, the implanted muscle constructs must have a means of anchoring to native bone so they may translate their contractile force production into movement. Our multiphasic SMUs meet this requirement via *in vitro* development of myotendinous junctions and entheses between their engineered muscle and bone/tendon components. These features give the constructs structural integrity similar to native muscles. Previous research from our lab has shown that similarly engineered multiphasic bone-ligament constructs reorganize and mature to develop native-like entheses after implantation *in vivo*.[24] Additionally, as a highly complex and metabolically demanding tissue, skeletal muscle relies on advanced vascular networks for blood perfusion and neurotization for maintenance of structure and contractile control. Previous research in our lab indicates that within a single week of implantation, our skeletal muscle constructs achieve vascularization and begin to develop innervation.[18]

Our laboratory has developed a rat model for creating and repairing acute VML by removing a longitudinal section, approximately one-third of the total width, from the lateral aspect of the tibialis anterior (TA) muscle. This model suits the geometry of our SMUs and, by leaving most of the distal TA tendon intact and drilling a bone tunnel in the lateral tibial head, it provides anchoring sites for the attachment of the bone-tendon anchors. Using our VML model in rats ($n=6$), we replaced $\sim$10% of the lost tissue volume with our SMUs and allowed for 28 days of recovery. The purpose of this study was to examine the potential of our SMUs to repair an acute 30% VML injury in 1 month and to examine advancement in the structure and function of our constructs with respect to muscle fiber size, vascularization, innervation, and construct force production. We hypothesized that the *in vivo* environment would promote integration of the SMU bone anchor into the native bone and the tendon anchor into native tendon and encourage advancement of the muscle phenotype beyond what was previously observed after a single week of implantation.

Materials and Methods

Animal model and animal care

Tissue engineering studies were conducted using soleus muscles and bone marrow from 120- to 150-g female Fischer 344 rats, obtained from Charles River Laboratories, Inc. (Wilmington, MA) and Harlan Laboratories (Haslett, MI). All animals were acclimated to our colony conditions for 1 week, that is, light cycle and temperature prior to any procedure. The animals were fed Purina Rodent Chow 5001 laboratory chow and water *ad libitum*. The harvested tissues were used as an allogenic cell source of muscle precursor cells and bone-marrow-derived stem cells for production of muscle and bone tissues that were later implanted into the host animals. The host animals were also female Fischer 344 rats. All surgical procedures were performed in an aseptic environment, with animals in a deep plane of anesthesia induced by isoflurane or intraperitoneal injections of sodium pentobarbital (65 mg/kg). Supplemental doses of pentobarbital were administered as required to maintain an adequate depth of anesthesia. All animal care and animal surgery procedures were in accordance with The Guide for Care and Use of Laboratory Animals[25] and the protocol was approved by the University Committee for the Use and Care of Animals.

Preparation of media

Unless otherwise indicated, all solutions and media were prepared and stored at 4°C prior to isolation and culture of cells and warmed to 37°C in a heated bead bath immediately prior to use. Muscle growth medium (M-GM) contained 30 mL F-12 Kaighn's Modification Nutrient Mixture (cat. No. 21127-022; Gibco BRL, Carlsbad, CA), 12.5 mL Dulbecco's modified Eagle's medium (DMEM; cat. No. 11995-065; Gibco BRL), 7.5 mL fetal bovine serum (FBS; cat. No. 10437-028; Gibco BRL), 2.4 ng/mL basic fibroblast growth factor (bFGF; cat. No. 100-18B; Peprotech, Rocky Hill, NJ), and 0.5 mL antibiotic-anti-mycotic (ABAM; cat. No. 15240-062; Gibco BRL). Muscle differentiation medium (M-DM) was composed of 33 mL M199 (cat. No. 11150-059; Gibco BRL), 14 mL DMEM, 3.3 mL FBS, 50 μL insulin-transferrin-selenium-X (cat. No. I1884; Sigma-Aldrich, St. Louis, MO), 0.5 mL ABAM, and 36.2 μL 50 μM ascorbic acid 2-phosphate. Transport medium (TM) consisting of Dulbecco's phosphate-buffered saline (DPBS [pH 7.2]; cat. No. 14190-144; Gibco BRL), with 2% ABAM, was used to transfer freshly isolated tissues from the surgical suite to the tissue culture facilities for isolation. Bone growth medium (B-GM) contained 40 mL DMEM and 10 mL FBS, supplemented with 1% ABAM, 6 ng/mL bFGF, and 5 ng/mL dexamethasone (cat. No. D4902; Sigma-Aldrich). Bone differentiation medium (B-DM) contained 46.5 mL DMEM and 3.5 mL FBS, supplemented with 1% ABAM, 0.13 mg/mL asc-2-phos, 0.05 mg/mL L-proline (cat. No. P0380; Sigma-Aldrich), and 5 ng/mL dexamethasone.

Preparation of construct dishes

Muscle constructs were fabricated in individual 60-mm plates, as described previously.[18,22] Each plate was coated with 5 mL Sylgard (type 184 silicon elastomer; Dow Chemical Corp., Midland, MI) and allowed to cure for 3 weeks prior to use. One to 7 days prior to use, each sylgard-coated plate was coated with laminin at 1 μg/cm^2 per plate (Natural Mouse Laminin, cat. No. 23017-015; Gibco BRL) suspended in 4 mL DPBS, and left to dry for 24–48 h. Residual salt crystals were dissolved and removed by rinsing the plates with 4 mL DPBS. The plates were then filled with 3 mL M-GM and decontaminated with UV light (wavelength 253.7 nm) for 60 min and placed in a 37°C/5% CO_2 incubator for up to 3 days prior to plating the muscle cells.

Preparation of tissue-engineered bone-tendon anchors

Bone marrow from Fischer 344 rats was removed under aseptic conditions. Isolated bone marrow cells were plated in 100-mm tissue culture plates (BD Falcon, Franklin Lakes, NJ) in 8 mL B-GM for 5 days and then passaged and replated. After four passages, the cells were plated in 100-mm tissue culture plates at a density of 1.3 million cells per plate. They were left to grow in 8 mL B-GM for 5 days before being shifted to B-DM for 2 days. At this stage, the confluent bone monolayers began to delaminate from the

tissue culture plate. The monolayers were collected, pinned in cylindrical forms into sylgard-coated dishes and fed B-DM, and left for 5–10 days prior to being cut into 5-mm sections to be used as engineered bone anchors for construct implantation. The anchors were then pinned onto the developing muscle monolayers.

Dissection of muscle and isolation of muscle cells

Both soleus muscles were removed under aseptic conditions and sterilized in 70% ethanol. Prior to dissociation, the muscles were incubated in 5 mL of TM for 5 min. The muscles were then minced using a razor blade, placed under ultraviolet light for 15 min in 15 mL of Ham's F12 (cat. No. 11765-047; Gibco BRL), and then added to a dissociation solution consisting of 32 U dispase (1.8 U/mg, cat. No. 17105-041; Gibco BRL) and 2390 U type IV collagenase (239 U/mg, cat. no. 17104-019; Gibco BRL) in 20 mL of Ham's f12 nutrient media. The mixture was then kept at 37°C with agitation for 90 min to allow the minced muscle to dissociate. The solution was then poured through a 100-μL filter and centrifuged. The dissociation solution was aspirated off and the cells were resuspended in M-GM.

Construct formation

The cell isolation mixture was plated in M-GM at a density of 400,000 cells per 60-mm plate. After the initial seeding, the plates were left undisturbed for 5 days, and subsequently fed M-GM every 2 days until they became ~70% confluent. At this point, the cells were lifted from the dish with 0.5 mL of 0.25% trypsin (Gibco BRL), mixed into M-GM, and seeded again at the same density. They were then fed M-GM every 2 days until the plates were 100% confluent and elongating myotubes began to form a network across the base of the plate. At this point, 5-mm tissue-engineered bone anchors were pinned onto the cell monolayers 2.5 cm apart and the media was changed to M-DM, which the plates were fed every 2 days. After approximately a week on M-DM, the monolayers were delaminated from the plates, rolling into cylindrical muscle constructs, held at length by the engineered bone anchors.

SMU contractile measurements

Contractile properties of the constructs were measured prior to implantation into host animals. The protocol for measuring contractility of engineered muscle constructs has been described previously.[26] Briefly, the pin on one end of the construct was freed from the Sylgard and attached to a force transducer with canning wax. For field stimulation of the entire construct, platinum wire electrodes were placed along either side of the SMU. The temperature of the construct was maintained at 37°C, using a heated aluminum platform. Passive baseline force was measured as the average baseline passive force preceding the onset of stimulation. Twitches were elicited using a single 2.5-ms pulse at 10, 30, 60, and 90 mA, whereas maximum tetanic force was determined using a 1-s train of 2.5-ms pulses at 90 mA and 10, 20, 40, 60, and 80 Hz. Data files for each peak twitch force and peak tetanic force trace were recorded and subsequently analyzed, using LabVIEW 2009 data acquisition software.

Surgical procedures

Each Fischer 344 SMU host rat was anesthetized using isofluorane. An incision was made along the left lower hindlimb exposing the TA, and a longitudinal cut was made to remove ~30% of the TA volume (Fig. 1A, B). A 0.9-mm tunnel was drilled into the proximal tendon insertion site on

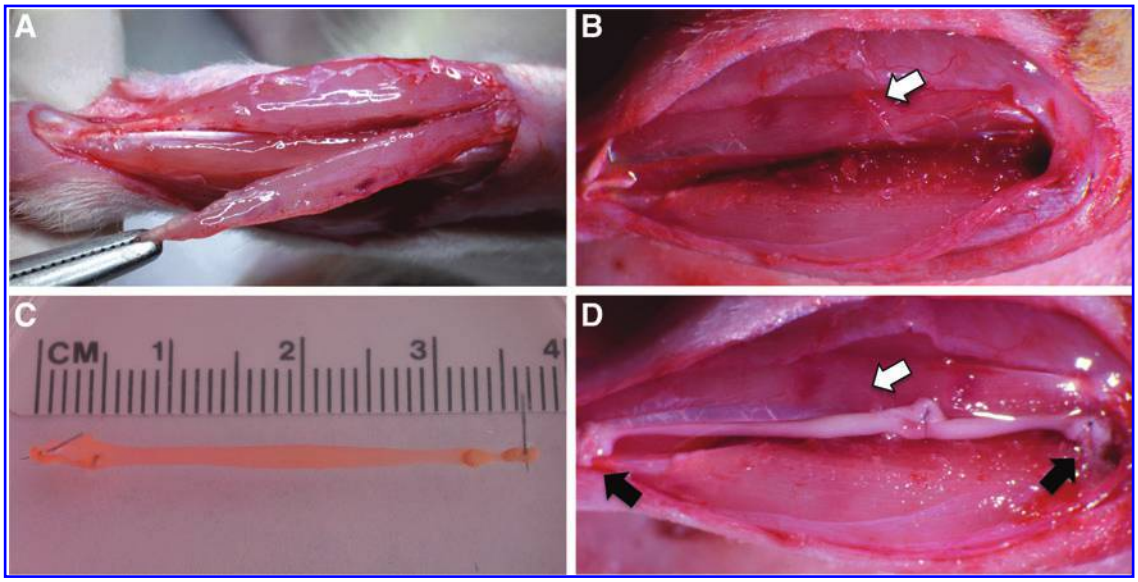

FIG. 1. A pictorial representation of the VML and SMU implantation procedure. **(A)** One-third of the left TA muscle was removed, **(B)** leaving an ~33% muscle volume deficit. **(C)** A single SMU **(D)** was implanted into the VML site, with one of its bone anchors inserted into a tibial bone tunnel and the other tendon end sutured to the distal TA tendon left from muscle volume removed. The tibial and distal TA tendon attachment sites are marked by black arrows in **D**. A branch of the peroneal nerve with its vasculature was isolated and sutured to the mid-belly of the SMU, marked by the white arrows in **B** and **D**. SMU, skeletal muscle unit; TA, tibialis anterior; VML, volumetric muscle loss. Color images available online at www.liebertpub.com/tea

the tibia, and the peroneal nerve distal to the innervation of the extensor digitorum longus was transected along with its associated vasculature, and routed to the area of VML. A single SMU (Fig. 1C) was then placed in the repair site, with one of its bone ends pulled into the tibial bone tunnel and sutured in place on the periosteum, and the other end of the construct sutured to the remaining distal tendon of the TA. The transected nerve branch was then sutured to the SMU using 9-0 suture (Fig. 1D). The surgical site was then closed with surgical staples and Carprofen was administered following each procedure at a dose of 5 mg/kg every 12 h for 48 h postsurgery. The staples were removed after 10 days.

TA contractile measurements

Following 28 days of recovery, *in vivo* contractile properties were measured as described by Larkin *et al.*[27] Briefly, the host and control rats were anesthetized with an injection of sodium pentobarbital (65 mg/kg) with supplemental injections given to maintain an adequate level of anesthesia throughout the procedures. Isometric contractile properties of the TA muscles were measured *in situ*. In anesthetized rats, the whole TA muscle was isolated from surrounding muscle and connective tissue using great care not to damage the nerve and/or blood vessels during the dissection. A 2–0 silk suture was tied around the distal tendon, and the tendon was severed. The animal was then placed on a temperature-controlled platform warmed to maintain body temperature at 37°C. The hindlimb was securely tied to a fixed post with wire at the knee. The distal tendon of the TA muscle was then tied to the lever arm of a servomotor (model 305B; Aurora Scientific). A continual drip of saline warmed to 37°C was administered to the TA muscle to maintain its temperature and to prevent desiccation. The muscle was activated by stimulation of the sciatic nerve using a bipolar platinum wire electrode. The voltage of single 0.2-ms stimulation pulses was adjusted to give a maximum isometric twitch. Subsequently, muscle length was adjusted to the optimal length (L_o) at which twitch force was maximal. With the muscle held at L_o, 300-ms trains of stimulus pulses were applied at increasing stimulation frequencies until the maximum isometric tetanic force (P_o) was achieved. Measures of L_o were taken and used to calculate functional CSA as described previously.[26]

After all force measurements were completed, muscles were removed, and deeply anesthetized rats were euthanized by administration of a pneumothorax and the TA muscles were trimmed of their tendons, blotted, and weighed. Muscle fiber length was calculated by multiplying L_o by a ratio of fiber length to TA muscle length described previously.[28] Total muscle CSA was calculated by dividing the muscle mass (mg) by the product of muscle fiber length (mm) and the density of mammalian skeletal muscle, 1.06 g/cm^2. Specific P_o (N/cm^2) was calculated by dividing P_o by total CSA for each muscle. Immediately after muscle mass was measured, muscles were coated in tissue-freezing medium (Triangle Biomedical Sciences, Durham, NC), frozen in isopentane cooled by dry ice, and stored at −80°C until analyzed for histology.

Histochemical and immunohistochemical analyses of SMU structure

Following measures of mechanical function, the frozen samples of repaired and contralateral TA were sectioned at 12 μm, mounted on Superfrost Plus microscopy slides, and used for histological analysis. Sections were stained for general morphology observations with hematoxylin and eosin (H&E). For immunohistochemical analysis, frozen sections were fixed with ice-cold methanol for 10 min and rinsed with DPBS. The sections were submerged for 15 min in 0.05% Triton X-100 (Sigma-Aldrich) in DPBS (PBST) and blocked with PBST containing 3% bovine serum albumin (PBST-S, cat. No. A2153-10g; Sigma-Aldrich) at room temperature. The sections were then incubated overnight at 4°C with the primary antibodies diluted in PBST-S. Immunofluorescent staining with specific antibodies was performed to detect the presence of myosin heavy chain (MF-20 mouse monoclonal antibody, 1:20 dilution, cat. No. ALD-58, obtained from the Developmental Studies Hybridoma Bank, Iowa City, IA), α-actinin (mouse monoclonal antibody, 1:200 dilution, cat. No. A7752; Sigma, St. Louis), collagen type 1 (rabbit polyclonal antibody, 5 mg/mL, cat. No. AB755P; Millipore, Billerica, MA), pan-axonal neurofilament (mouse monoclonal antibody, 1:300 dilution, cat. No. SMI-312R; Covance, Inc., Princeton NJ), CD-31 (mouse monoclonal antibody, 1:100 dilution, cat. No. ab24590; Abcam, Cambridge, MA), paxillin (rabbit polyclonal antibody, 1:100 dilution, cat. No. ab2264; Abcam), α-bungarotoxin (1:20 dilution, cat. No. B-1601; Molecular Probes, Carlsbad, CA), polymorphonuclear leukocytes (PMNs; rabbit polyclonal antibody, cat. No. AIAD31140, 1:100 dilution; Accurate Chemical, Westbury, NY), F4/80 (biotin-conjugated mouse monoclonal antibody, 1:200 dilution, cat. No. MCA497B; AbD Serotec, Raleigh, NC), and fibroblast specific protein 1 (FSP1; rabbit polyclonal antibody, 1:200 dilution; Neomarkers, Fremont, CA). Following three washes in PBST, the sections were incubated in 1:500 dilutions of with Alexa Fluor anti-mouse, anti-chicken, or anti-rabbit antibodies (Life Technologies, Carlsbad, CA) for 3 h at room temperature. Following three washes in PBST, the sections were fixed in Prolong Gold with DAPI and coverslipped. The sections were examined and photographed with an Olympus microscope and cross-sections of the constructs were analyzed using the Image J software package.

Statistical analysis

Values are presented as mean ± standard error. Measurements of significant differences between means were performed using JMP statistical analysis software. Means were compared using one-way analysis of variance tests with Tukey *post-hoc* analyses. Differences were considered significant at $p < 0.05$.

Results

Muscle masses and contractile properties

Following a 28-day recovery period, the body masses and the repaired and contralateral TA muscle masses were compared to determine the effects the SMUs had on overall TA muscle mass and health of the animal. The average body masses of the rats from the control, acute VML, and repaired TA groups were 170 ± 2.4, 166 ± 2.8, and 170 ± 3.7 g, respectively, and were not statistically different (Fig. 2A), indicating that the graft and surgical procedure had no

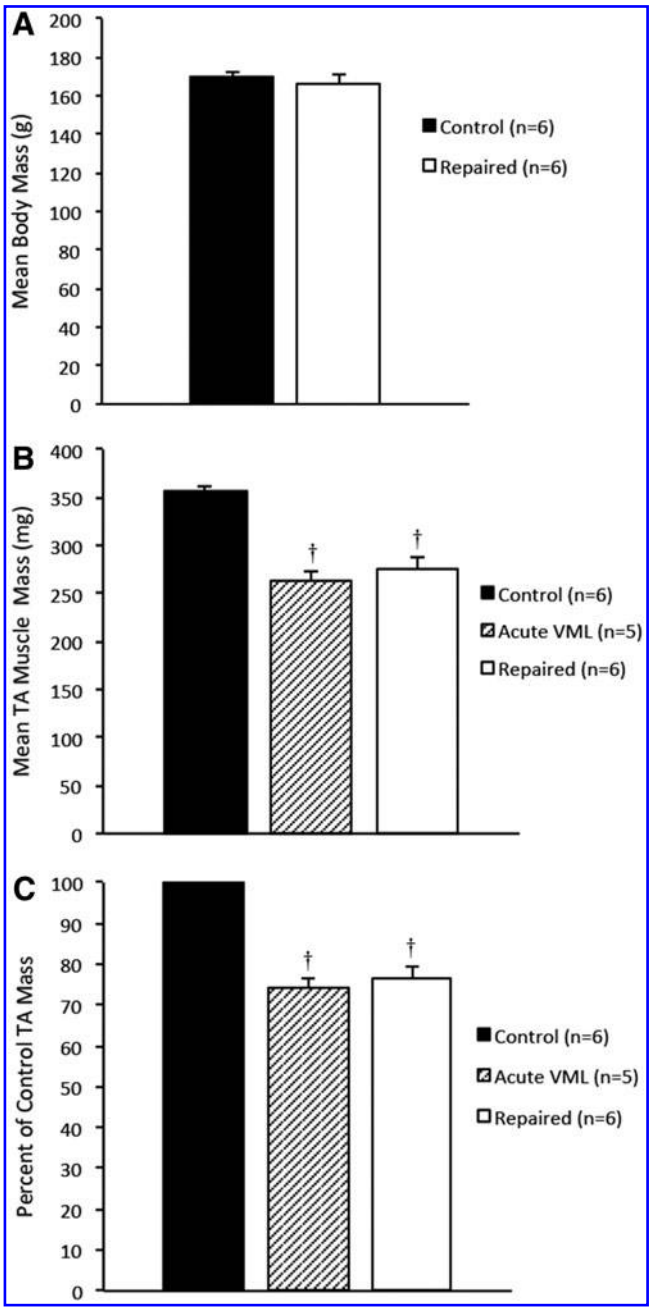

FIG. 2. **(A)** A comparison of the average animal body masses in control, acute VML, and repaired VML groups shows no significant differences, indicating that direct comparisons of TA mass and force production can be drawn. **(B)** A comparison of TA masses shows a significant mass deficit in both the acute VML and the repaired TA groups in comparison to the control group ($p < 0.0001$ and $p = 0.0002$, respectively). The difference in average TA mass between these groups was not significant, indicating that the SMUs did not appreciably restore muscle volume to the repaired TAs in 28 days. **(C)** Normalized to the average control TA mass, the damage to the acute VML TAs constituted a $26\% \pm 2.1\%$ mass deficit and the repaired TAs were found to have a $22\% \pm 2.8\%$ mass deficit. Error bars indicate standard error. †Statistical difference from control group.

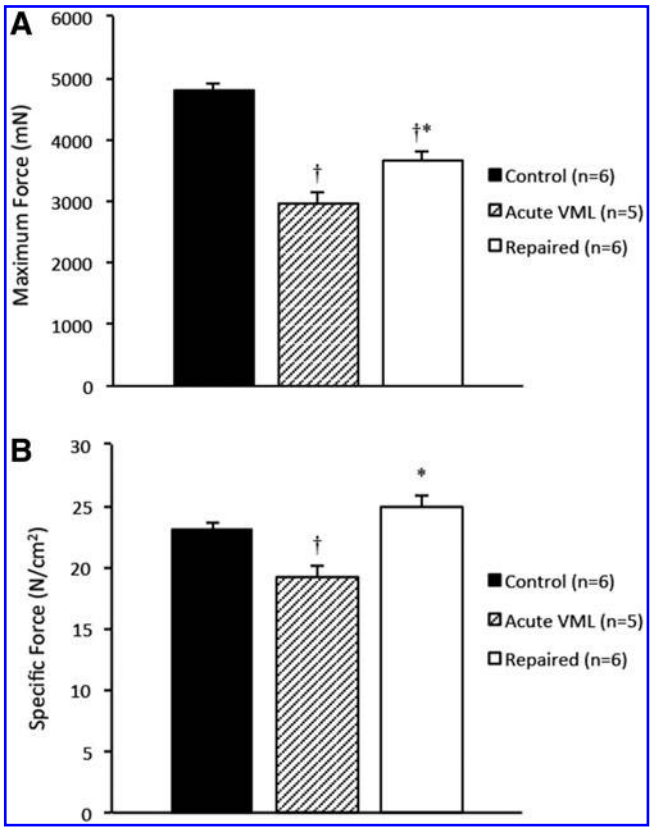

FIG. 3. **(A)** A comparison of the average maximum forces produced by the repaired TAs and the control TAs reveals a $24\% \pm 3.0\%$ force production deficit ($p = 0.0012$), indicating that the SMUs did not fully restore force production to the repaired TAs after 28 days of recovery. The acute VML group suffered a $38\% \pm 3.5\%$ force production deficit ($p < 0.0001$), which may be largely attributed to hemorrhaging and damage from the VML procedure. **(B)** Specific forces for each group indicate that the control and repaired TAs fall within the expected range for healthy skeletal muscle, while the acute VML group produced a decreased specific force ($p = 0.0040$) likely due to the compromised muscle integrity. Error bars indicate standard error. †Statistical difference from control group; *statistical difference from acute VML group.

impact on the growth of the animals. The average TA masses of the control, acute VML, and repaired TA groups were 357 ± 5.2, 264 ± 7.5, and 276 ± 10.5 mg, respectively (Fig. 2B). The difference between the average control TA mass and the average repaired and acute VML TA masses was statistically significant ($p = 0.0002$ and $p < 0.0001$, respectively). Normalized to the average control TA mass, the acute VML TAs had an average mass deficit of $26\% \pm 2.1\%$, while the repaired TAs had an average mass deficit of $22\% \pm 2.8\%$ of the average control TA mass (Fig. 2C). The average masses of the repaired and acute VML TAs were not significantly different.

The SMUs had a mean preimplantation force of 121 ± 9.6 μN. Following the recovery period, the SMUs were thoroughly integrated into the host TAs and could not be separated and force-tested independent of the host muscle without damaging the construct tissue and compromising the contractile data. The maximum forces produced by the

repaired muscles averaged 24% ± 3.0% less than those produced by the control muscles ($p = 0.0012$), indicating that the SMUs did not fully restore maximum force production to the injured TAs (Fig. 3A). The specific forces of both repaired and control TAs were calculated and the difference in specific forces between the groups was not found to be significant (Fig. 3B). This indicates that the graft did not adversely affect the function of the repaired TA muscle.

Morphology of muscle constructs

H&E staining of the repaired and control TA sections was performed to analyze the general morphology of the SMUs after 28 days of recovery (Fig. 4A). The CSA of the repaired tissue was measured and found to be 1.24% ± 0.03% of the CSA of the muscle removed.

In addition, it was noted that the myogenic cells within the SMUs developed into small but distinct muscle fibers at an average of 181 ± 26 fibers per graft. The CSAs of the newly formed muscle fibers found within the grafted area were 118 ± 6 μm^2, or 8.0% of the mean CSA of control native TA fibers, which averaged 1473 ± 45 μm^2 (Fig. 4C). The difference between the average graft and native muscle fiber CSA was statistically significant ($p < 0.0001$).

Immunohistochemistry

Immunostaining was used to visualize the presence of myosin heavy chain and laminin in the SMUs (Fig. 4B). Myosin heavy chain content confirmed the identity of these structures as muscle fibers, while immunostaining for laminin indicated that each SMU fiber has a laminin-rich extracellular matrix, much like the endomysium surrounding individual native fibers. Immunostaining for macrophage and granulocyte markers (F4/80 and PMN, respectively) was performed to determine the presence of these cells in the graft region (Fig. 4A); however, no evidence of immune cell infiltration was observed (data not shown). Immunostaining for the fibroblast marker FSP1 indicated that a number of cells in the area of regeneration are fibroblasts (Fig. 4D).

Immunostaining for α-actinin (Fig. 5A) indicated that the construct fibers are aligned along the length of the SMUs and developed advanced sarcomeric organization (Fig. 5B), similar to that found in native muscle. Immunostaining for CD-31 indicated the presence of an advanced capillary network throughout the construct tissue, similar to that in native skeletal muscle (Fig. 6A, B). Immunostaining for paxillin (Fig. 7) at the junction between muscle fibers (myosin heavy chain) and tendon (Collagen 1) showed the development of myotendinous junctions in the implanted SMUs.

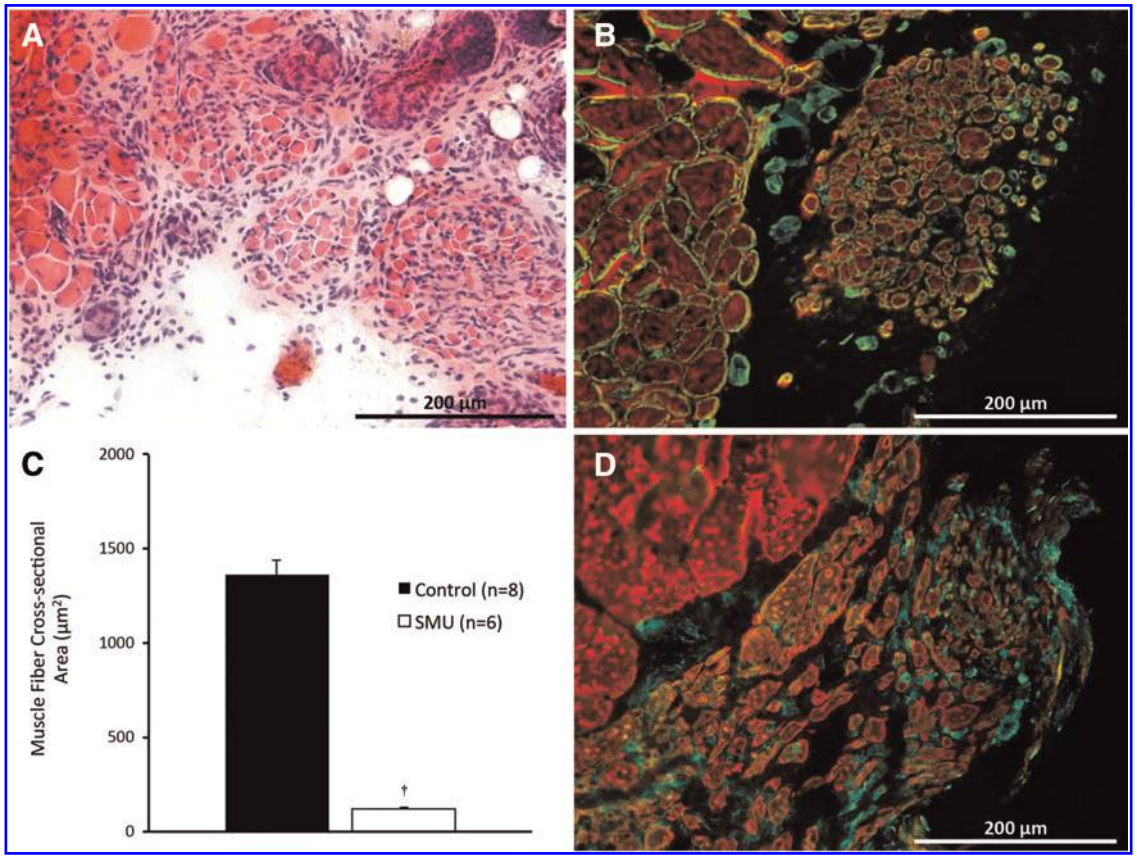

FIG. 4. **(A)** Cross-sectional area (CSA) analysis of construct morphology indicates that after 30 days *in vivo*, the SMUs developed small but defined muscle fibers. **(B)** The construct fibers featured laminin-rich extracellular matrices (Laminin, green) and expressed myosin heavy chain (MF-20, red). **(C)** Analysis of the CSAs of the construct ($n = 6$ constructs) and native control TA ($n = 8$) fibers indicates that the construct fibers' average CSA is 118 ± 6 μm^2, or 8.0% of the average CSA of the native fibers in the control TAs ($p < 0.0001$). **(D)** Staining for fibroblast specific protein 1 (FSP1, green) indicates that the numerous cells near the graft muscle fibers (MF-20, red) are fibroblasts. Error bars indicate standard error. †Statistical difference from the native muscle fibers. Color images available online at www.liebertpub.com/tea

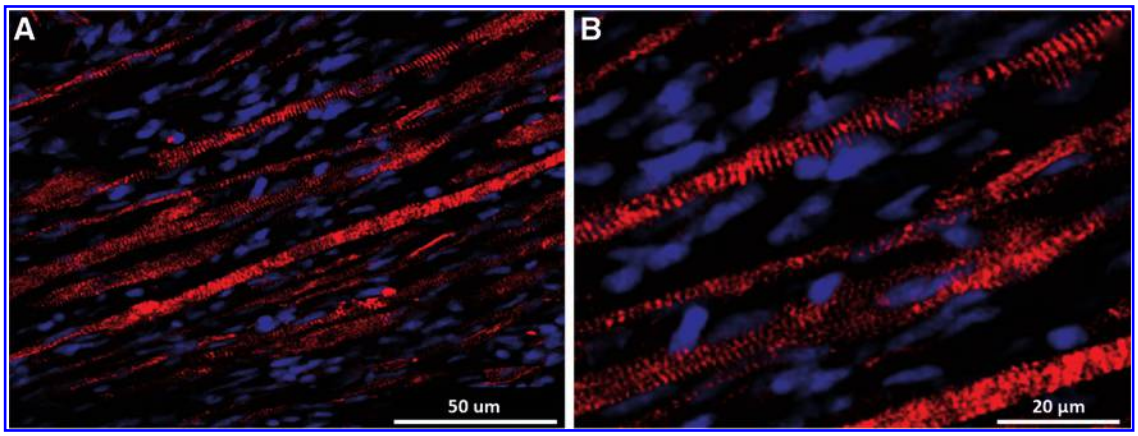

FIG. 5. **(A)** Immunohistochemical analysis of longitudinal SMU sections with an anti-α-actinin antibody indicates that after 28 days *in vivo*, the SMU muscle fibers are closely aligned along the length of the construct, mimicking the organization of native muscle tissue. **(B)** The same image at a greater magnification indicates that the SMU muscle fibers also developed advanced sarcomeric structure. Color images available online at www.liebertpub.com/tea

Immunostaining for neurofilament and costaining with tetramethylrhodamine-conjugated α-bungarotoxin indicated the presence of numerous neural branches throughout the graft tissue originating from the grafted nerve and traversing along the length of the construct. High concentrations of neuromuscular junctions were found in the region where the grafted nerve interfaces with the SMUs (Fig. 8A). Colocalization of the α-bungarotoxin and neurofilament stains indicated that the nerve branches terminate at neuromuscular junctions, forming a neuromuscular interface in the construct tissue (Fig. 8B).

Bone tunnel repair

After removal of the TA muscles, the tibial bones were collected and cleaned for inspection of the bone tunnels. Figure 9 shows a comparison of an unaltered control tibia (Fig. 9A), an unrepaired tibia showing the location of the 0.9-mm tibial head bone tunnel (Fig. 9B), and repaired tibia with the bone tunnel fully healed (Fig. 9C). Five of the six repaired tibias showed complete healing of the tibial head and integration of the proximal SMU bone anchor into the native bone tissue. The sixth tibia showed only partial healing of the bone tunnel during recovery (Fig. 9D); however, this did not appear to impact development of the SMUs.

Discussion

The purpose of this study was to examine the effects of *in vivo* implantation on the maturation of our SMUs and to evaluate their potential to treat VML. We hypothesized that the 28-day implantation period would promote advancement of the construct muscle phenotype toward that of an adult skeletal muscle, including increases in fiber size, sarcomere organization, and vascular/neural interfacing. We also hypothesized that the SMUs would partially restore lost muscle volume and begin to contribute to overall muscle force production.

After 28 days of exposure to the *in vivo* environment, our constructs exhibited structural advancements from their *in vitro* state. Perhaps the most significant alteration to the SMU phenotype was the formation of distinct and uniaxial

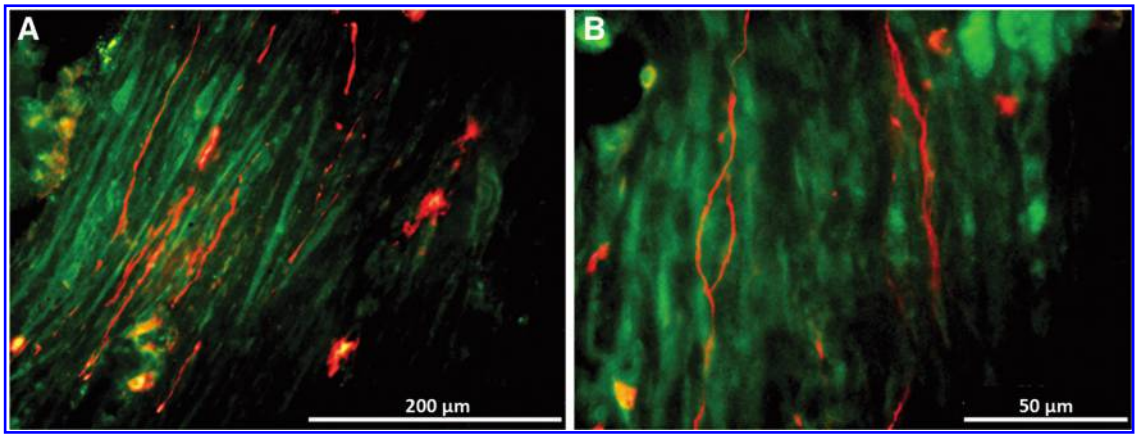

FIG. 6. **(A, B)** Immunohistochemical staining for CD-31 (red) and Collagen 1 (green) indicates the presence of a well-developed capillary network throughout the engineered muscle tissue. As in native muscle, most of the vasculature is aligned with the muscle fibers. Color images available online at www.liebertpub.com/tea

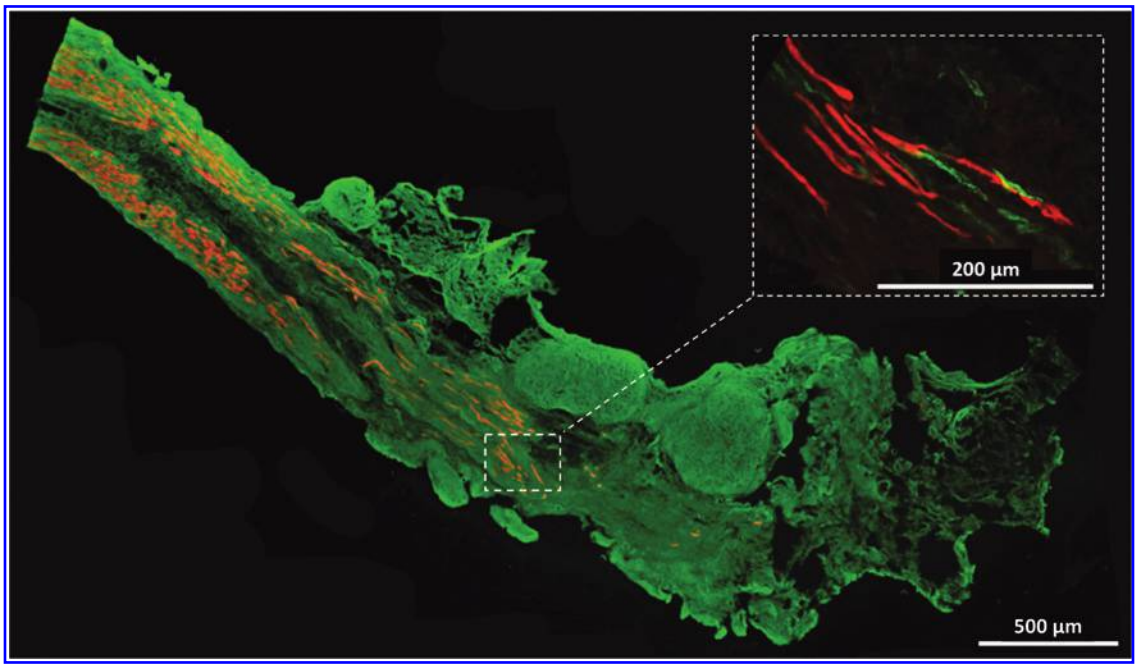

FIG. 7. Immunohistochemical staining for myosin heavy chain (red) and Collagen type 1 (green) shows the structure of the SMU muscle to tendon interface. Inset: The presence of paxillin (green) at this interface and its colocalization with the graft muscle fibers (red) demonstrate the similarity of this interface to a native myotendinous junction. Color images available online at www.liebertpub.com/tea

aligned muscle fibers encased in an extensive extracellular matrix, similar in structure to native skeletal muscle. The fiber alignment marks a significant advancement in the structural organization beyond that observed in many other skeletal muscle tissue engineering approaches, which demonstrate *in vivo* increases in graft muscle content, but fall short of developing true, aligned muscle fibers. Considerable research effort has been directed toward promoting *in vitro* fiber alignment in engineered muscle tissue. These methods include utilizing scaffolds with aligned pores[29] or microgrooves[30] and culture bases with aligned fibronectin stripes[31] to encourage common orientation of developing myotubes *in vitro*. While these strategies have found considerable success, our SMUs also exhibit fiber alignment without the limitations posed by scaffolds, thus offering an alternative approach for skeletal muscle engineering. Our scaffoldless technology prevents stress-shielding of the engineered muscle fibers, allowing for uniaxial loading of the SMUs. This encourages proper fiber alignment and optimizes force production and transmission to tendon and bone.

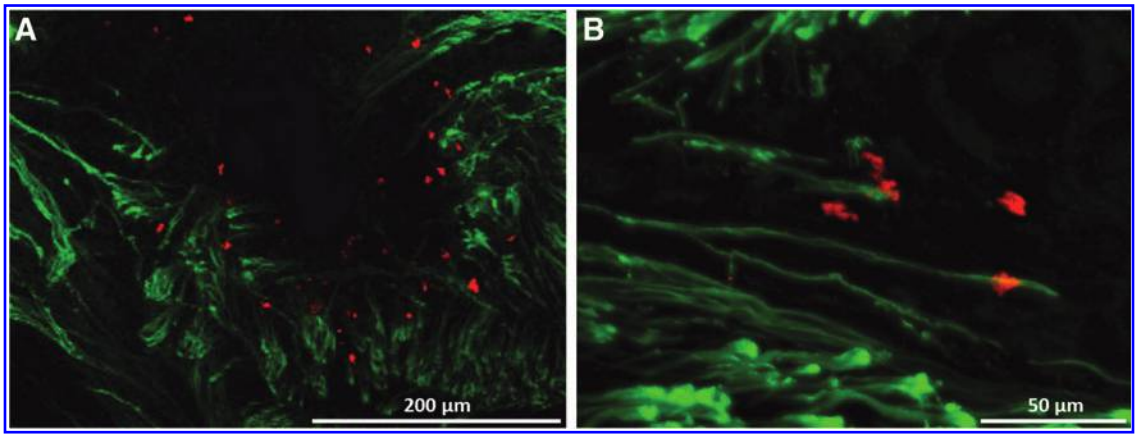

FIG. 8. Immunohistochemical staining for pan-axonal neurofilament (green) and acetylcholine receptors (alpha-bungarotoxin, red) indicates that after 28 days of implantation, the engineered muscle becomes highly innervated and forms neuromuscular junctions. **(A)** Regions in the engineered muscle near the grafted nerve show high densities of colocalized motor neurons and acetylcholine receptor clusters, indicating development of a neuromuscular interface between the host and the graft muscle. **(B)** These neuromuscular junctions were found at the termini of neural branches within the SMUs. Color images available online at www.liebertpub.com/tea

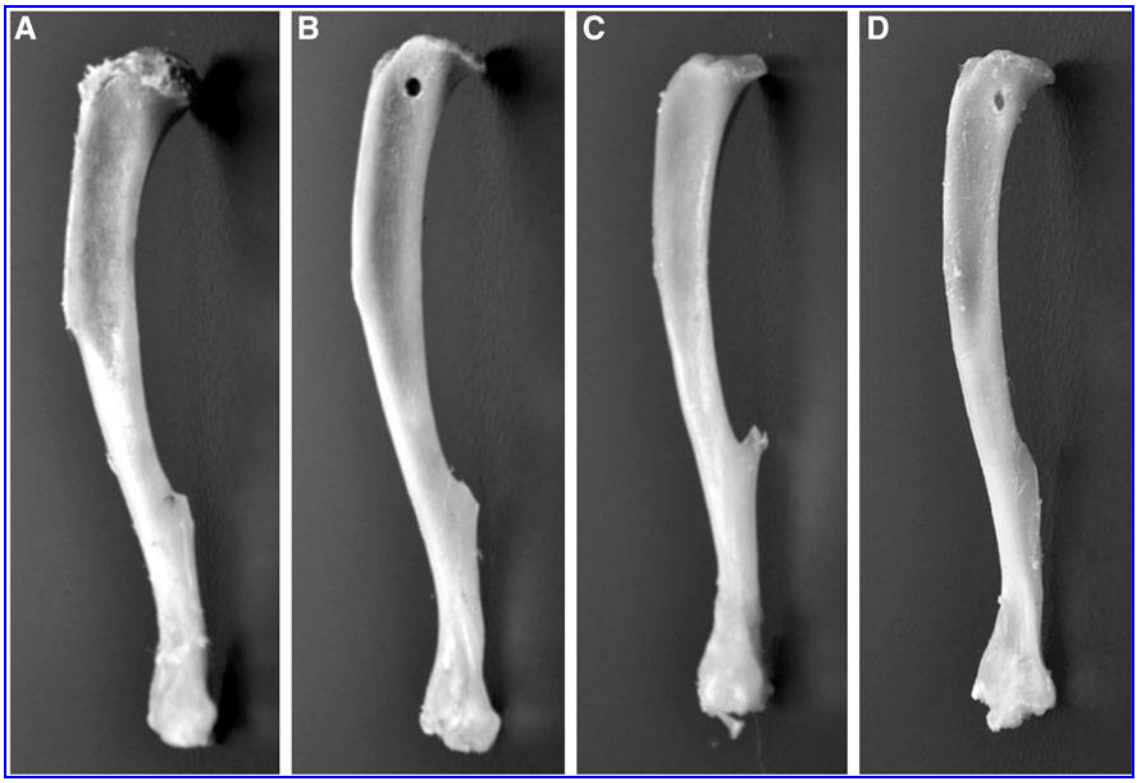

FIG. 9. Photographs of **(A)** an unaltered left tibia, **(B)** a tibia with a 9-mm-diameter bone tunnel in the tibial head for anchoring an SMU, **(C)** and a tibia from a rat with an implanted SMU show that the bone anchor of the SMU fully repaired the 9-mm surgical anchor hole and integrated into the native tissue of the tibial head. **(D)** A photograph of one of the repaired tibias shows incomplete healing of the bone tunnel.

Analysis of the explanted TAs did not indicate any evidence of immune response to the grafts at the time of examination. This was expected, as no immune response was found in previous engineered muscle implantation studies after one week of *in vivo* development. Numerous fibroblasts were found dispersed among the regenerating muscle fibers, which may indicate remodeling of the graft extracellular matrix to accommodate the developing muscle fibers. We hypothesize that these fibroblasts originated from the graft tissue, which is partially composed of fibroblasts prior to implantation. The nature of SMU development and remodeling with respect to native cell infiltration and turnover will be examined in future studies.

Examination of the repaired tibial bone indicated that the bone-tendon anchors of our SMUs integrated into the native bone of the tibial heads as they healed, forming entheses with the native bone tissue and myotendinous junctions with the engineered muscle. The development of these tendon-like interfaces between the host and graft tissues is significant to the application of our skeletal muscle engineering technology; rather than repairing only sections of damaged muscle, our SMUs can also provide restoration of damaged bone-tendon-muscle interfaces. Further, because they develop these interfaces, mimicking the gross structure of native muscles, they are able to effectively transmit force between anchoring structures as native muscles do. This would potentially allow the SMUs to be used for full muscle replacement in addition to muscle repair.

Promising research has been performed on *in vitro* neurotization and neuromuscular interfacing of engineered muscle[19,32] and *in vivo* work had demonstrated the necessity of innervation to the functional advancement of engineered muscle tissue.[33] Of particular interest is the innervation and formation of neuromuscular junctions, an obstacle to tissue engineering strategies for muscle repair, and a critical step for contractile control of engineered muscle graft tissue.[34] Our immunohistochemical stains show numerous nerve fibers branching from the grafted nerve into our engineered muscle, with individual nerve branches extending throughout the grafted region and terminating at clusters of acetylcholine receptors, demonstrating the *in vivo* development of neuromuscular junctions within the SMUs.

Though recent research on the innervation of graft muscle tissue has shown development of neuromuscular junctions after 8 weeks, complete restoration of muscle function was not achieved even after 12 weeks.[34] Past studies in our lab have also demonstrated that reinnervation of the rat medial gastrocnemius muscle after denervation is an extensive process that may require over 3 months before maximum recovery is achieved.[35] Thus, despite the promising innervation and neuromuscular junction formation observed in our SMUs, it is likely that their neuromuscular interfaces had not yet fully matured after only 28 days *in vivo*. We hypothesize that given greater time to recover, the developing muscle fibers within our SMUs will increase their size and strength toward that of native muscle fibers. This study was intended to assess the survival and early development of

our SMUs when used to treat VML, while ongoing studies with recovery times of 3 months and beyond will focus on the maturation of the SMU neuromuscular systems and their subsequent functional contributions to repaired muscles.

In conclusion, though our SMUs did not fully restore muscle mass or force production in our VML model, they survived *in vivo* and exhibited significant advancement in phenotype, indicating that further investigation of their use for partial or even entire small muscle repair is warranted. Future studies will focus on longer implantation durations, larger tissue replacement volumes, and entire muscle replacements.

Acknowledgments

The authors would like to acknowledge Jessica Dou for her technical assistance and the University of Michigan for providing internal funding for this research.

Disclosure Statement

No competing financial interests exist.

References

1. Mertens, J.P., Sugg, K.B., Lee, J.D., and Larkin, L.M. Engineering muscle constructs for the creation of functional engineered musculoskeletal tissue. Regen Med **9,** 89, 2014.
2. Grogan, B.F., and Hsu, J.R.; Skeletal Trauma Research Consortium. Volumetric muscle loss. J Am Acad Orthop Surg **19 Suppl 1,** S35, 2011.
3. Tedesco, F.S., Dellavalle, A., Diaz-Manera, J., Messina, G., and Cossu, G. Repairing skeletal muscle: regenerative potential of skeletal muscle stem cells. J Clin Invest **120,** 11, 2010.
4. Terzis, J.K., and Kostopoulos, V.K. Free muscle transfer in posttraumatic plexopathies: part 1: the shoulder. Ann Plast Surg **65,** 312, 2010.
5. Hierner, R., Reynders-Frederix, P., Bellemans, J., Stuyck, J., and Peeters, W. Free myocutaneous latissimus dorsi flap transfer in total knee arthroplasty. J Plast Reconstr Aesthet Surg **62,** 1692, 2009.
6. Romeo, M., *et al.* An anterior-lateral thigh perforator flap on a recipient brachial-radial vein graft for complex wound reconstruction: a case report. Microsurgery **29,** 495, 2009.
7. Terzis, J.K., and Kostopoulos, V.K. Free muscle transfer in posttraumatic plexopathies: part III. The hand. Plast Reconstr Surg **124,** 1225, 2009.
8. Fan, C., *et al.* Functional reconstruction of traumatic loss of flexors in forearm with gastrocnemius myocutaneous flap transfer. Microsurgery **28,** 71, 2008.
9. Lin, C.-H., Lin, Y.-T., Yeh, J.-T., and Chen, C.-T. Free functioning muscle transfer for lower extremity posttraumatic composite structure and functional defect. Plast Reconstr Surg **119,** 2118, 2007.
10. Vandenburgh, H.H., Karlisch, P., and Farr, L. Maintenance of highly contractile tissue-cultured avian skeletal myotubes in collagen gel. Vitro Cell Dev Biol J Tissue Cult Assoc **24,** 166, 1988.
11. Dennis, R.G., Kosnik, P.E., Gilbert, M.E., and Faulkner, J.A. Excitability and contractility of skeletal muscle engineered from primary cultures and cell lines. Am J Physiol Cell Physiol **280,** C288, 2001.
12. Dennis, R.G., and Kosnik, P.E., 2nd. Excitability and isometric contractile properties of mammalian skeletal muscle constructs engineered *in vitro*. In Vitro Cell Dev Biol Anim **36,** 327, 2000.
13. Deans, T.L., and Elisseeff, J.H. Stem cells in musculoskeletal engineered tissue. Curr Opin Biotechnol **20,** 537, 2009.
14. Liao, H., and Zhou, G.-Q. Development and progress of engineering of skeletal muscle tissue. Tissue Eng Part B Rev **15,** 319, 2009.
15. Payumo, F.C., *et al.* Tissue engineering skeletal muscle for orthopaedic applications. Clin Orthop Relat Res S228, 2002.
16. Scime, A., Caron, A.Z., and Grenier, G. Advances in myogenic cell transplantation and skeletal muscle tissue engineering. Front Biosci (Landmark Ed) **14,** 3012, 2009.
17. Turner, N.J., and Badylak, S.F. Regeneration of skeletal muscle. Cell Tissue Res **347,** 759, 2012.
18. Williams, M.L., Kostrominova, T.Y., Arruda, E.M., and Larkin, L.M. Effect of implantation on engineered skeletal muscle constructs. J Tissue Eng Regen Med **7,** 434, 2013.
19. Larkin, L.M., Van der Meulen, J.H., Dennis, R.G., and Kennedy, J.B. Functional evaluation of nerve-skeletal muscle constructs engineered *in vitro*. In Vitro Cell Dev Biol Anim **42,** 75, 2006.
20. Baker, E.L., Dennis, R.G., and Larkin, L.M. Glucose transporter content and glucose uptake in skeletal muscle constructs engineered *in vitro*. In Vitro Cell Dev Biol Anim **39,** 434, 2003.
21. Kostrominova, T.Y., Calve, S., Arruda, E.M., and Larkin, L.M. Ultrastructure of myotendinous junctions in tendon-skeletal muscle constructs engineered *in vitro*. Histol Histopathol **24,** 541, 2009.
22. Larkin, L.M., Calve, S., Kostrominova, T.Y., and Arruda, E.M. Structure and functional evaluation of tendon-skeletal muscle constructs engineered *in vitro*. Tissue Eng **12,** 3149, 2006.
23. Weist, M.R., *et al.* TGF-β1 enhances contractility in engineered skeletal muscle. J Tissue Eng Regen Med **7,** 562, 2013.
24. Ma, J., *et al.* Three-dimensional engineered bone-ligament-bone constructs for anterior cruciate ligament replacement. Tissue Eng Part A **18,** 103, 2012.
25. National Research Council. Guide for the Care and Use of Laboratory Animals, Eighth Edition. The National Academies Press. Washington D.C., 2011.
26. Larkin, L.M., Kuzon, W.M., Jr., Supiano, M.A., Galecki, A., and Halter, J.B. Effect of age and neurovascular grafting on the mechanical function of medial gastrocnemius muscles of Fischer 344 rats. J Gerontol A Biol Sci Med Sci **53,** B252, 1998.
27. Larkin, L.M., *et al.* Skeletal muscle weakness due to deficiency of CuZn-superoxide dismutase is associated with loss of functional innervation. Am J Physiol Regul Integr Comp Physiol **301,** R1400, 2011.
28. Burkholder, T.J., Fingado, B., Baron, S., and Lieber, R.L. Relationship between muscle fiber types and sizes and muscle architectural properties in the mouse hindlimb. J Morphol **221,** 177, 1994.
29. Zhao, W., *et al.* Diaphragmatic muscle reconstruction with an aligned electrospun poly(ε-caprolactone)/collagen hybrid scaffold. Biomaterials **34,** 8235, 2013.
30. Hosseini, V., *et al.* Engineered contractile skeletal muscle tissue on a microgrooved methacrylated gelatin substrate. Tissue Eng Part A **18,** 2453, 2012.

31. Sun, Y., Duffy, R., Lee, A., and Feinberg, A.W. Optimizing the structure and contractility of engineered skeletal muscle thin films. Acta Biomater **9,** 7885, 2013.
32. Das, M., Rumsey, J.W., Bhargava, N., Stancescu, M., and Hickman, J.J. A defined long-term *in vitro* tissue engineered model of neuromuscular junctions. Biomaterials **31,** 4880, 2010.
33. Dhawan, V., Lytle, I.F., Dow, D.E., Huang, Y.-C., and Brown, D.L. Neurotization improves contractile forces of tissue-engineered skeletal muscle. Tissue Eng **13,** 2813, 2007.
34. Kang, S.-B., Olson, J.L., Atala, A., and Yoo, J.J. Functional recovery of completely denervated muscle: implications for innervation of tissue-engineered muscle. Tissue Eng Part A **18,** 1912, 2012.
35. Larkin, L.M., Kuzon, W.M., and Halter, J.B. Effects of age and nerve-repair grafts on reinnervation and fiber type distribution of rat medial gastrocnemius muscles. Mech Ageing Dev **124,** 653, 2003.

Address correspondence to:
Lisa M. Larkin, PhD
Department of Molecular and Integrative Physiology
University of Michigan
Biomedical Science Research Building (BSRB)
109 Zina Pitcher Place, Room #2025
Ann Arbor, MI 48109-2200

E-mail: llarkin@umich.edu

Received: January 22, 2014
Accepted: April 24, 2014
Online Publication Date: June 23, 2014

This article has been cited by:

1. Brittany L. Rodriguez, Lisa M. Larkin. Functional three-dimensional scaffolds for skeletal muscle tissue engineering 279-304. [Crossref]
2. Sarah M. Greising, Jessica C. Rivera, Stephen M. Goldman, Alain Watts, Carlos A. Aguilar, Benjamin T. Corona. 2017. Unwavering Pathobiology of Volumetric Muscle Loss Injury. *Scientific Reports* **7**:1. . [Crossref]
3. Syverud Brian C., Lin Eric, Nagrath Sunitha, Larkin Lisa M.. Label-Free, High-Throughput Purification of Satellite Cells Using Microfluidic Inertial Separation. *Tissue Engineering Part C: Methods*, ahead of print. [Abstract] [Full Text HTML] [Full Text PDF] [Full Text PDF with Links]
4. Syverud Brian C., Mycek Mary-Ann, Larkin Lisa M.. 2017. Quantitative, Label-Free Evaluation of Tissue-Engineered Skeletal Muscle Through Multiphoton Microscopy. *Tissue Engineering Part C: Methods* **23**:10, 616-626. [Abstract] [Full Text HTML] [Full Text PDF] [Full Text PDF with Links]
5. Mr. Brian C Syverud, Mr. Eric Lin, Dr. Sunitha Nagrath, Dr. Lisa Marie Larkin. Label-Free, High-Throughput Purification of Satellite Cells Using Microfluidic Inertial Separation. *Tissue Engineering Part C: Methods* **0**:ja. . [Abstract] [Full Text PDF] [Full Text PDF with Links]
6. Marco Quarta, Melinda Cromie, Robert Chacon, Justin Blonigan, Victor Garcia, Igor Akimenko, Mark Hamer, Patrick Paine, Merel Stok, Joseph B. Shrager, Thomas A. Rando. 2017. Bioengineered constructs combined with exercise enhance stem cell-mediated treatment of volumetric muscle loss. *Nature Communications* **8**, 15613. [Crossref]
7. Passipieri J.A., Baker H.B., Siriwardane Mevan, Ellenburg Mary D., Vadhavkar Manasi, Saul Justin M., Tomblyn Seth, Burnett Luke, Christ George J.. 2017. Keratin Hydrogel Enhances In Vivo Skeletal Muscle Function in a Rat Model of Volumetric Muscle Loss. *Tissue Engineering Part A* **23**:11-12, 556-571. [Abstract] [Full Text HTML] [Full Text PDF] [Full Text PDF with Links]
8. Jorge A. Uquillas, Settimio Pacelli, Shuichiro Kobayashi, Sebastián Uquillas. Musculoskeletal Tissue Engineering: Tendon, Ligament, and Skeletal Muscle Replacement and Repair 465-523. [Crossref]
9. John B. Scott, Catherine L. Ward, Benjamin T. Corona, Michael R. Deschenes, Benjamin S. Harrison, Justin M. Saul, George J. Christ. 2017. Achieving Acetylcholine Receptor Clustering in Tissue-Engineered Skeletal Muscle Constructs In vitro through a Materials-Directed Agrin Delivery Approach. *Frontiers in Pharmacology* **7**. . [Crossref]
10. Ken Muneoka, Eva Lai, Robert J. Christy, Jon E. Mogford. Limb Regrowth and Tissue Engineering Alternatives 213-236. [Crossref]
11. I. Y. Shadrin, A. Khodabukus, N. Bursac. 2016. Striated muscle function, regeneration, and repair. *Cellular and Molecular Life Sciences* **73**:22, 4175-4202. [Crossref]
12. Benjamin T. Corona, Sarah M. Greising. 2016. Challenges to acellular biological scaffold mediated skeletal muscle tissue regeneration. *Biomaterials* **104**, 238-246. [Crossref]
13. John T. Kim, Benjamin M. Kasukonis, Lemuel A. Brown, Tyrone A. Washington, Jeffrey C. Wolchok. 2016. Recovery from volumetric muscle loss injury: A comparison between young and aged rats. *Experimental Gerontology* **83**, 37-46. [Crossref]
14. Syverud Brian C., VanDusen Keith W., Larkin Lisa M.. 2016. Effects of Dexamethasone on Satellite Cells and Tissue Engineered Skeletal Muscle Units. *Tissue Engineering Part A* **22**:5-6, 480-489. [Abstract] [Full Text HTML] [Full Text PDF] [Full Text PDF with Links]
15. Nenad Bursac, Mark Juhas, Thomas A. Rando. 2015. Synergizing Engineering and Biology to Treat and Model Skeletal Muscle Injury and Disease. *Annual Review of Biomedical Engineering* **17**:1, 217-242. [Crossref]
16. Shangwu Chen, Tomoko Nakamoto, Naoki Kawazoe, Guoping Chen. 2015. Engineering multi-layered skeletal muscle tissue by using 3D microgrooved collagen scaffolds. *Biomaterials* **73**, 23-31. [Crossref]
17. Jonathan M. Grasman, Duc M. Do, Raymond L. Page, George D. Pins. 2015. Rapid release of growth factors regenerates force output in volumetric muscle loss injuries. *Biomaterials* **72**, 49-60. [Crossref]
18. Amit Aurora, Janet L. Roe, Benjamin T. Corona, Thomas J. Walters. 2015. An acellular biologic scaffold does not regenerate appreciable de novo muscle tissue in rat models of volumetric muscle loss injury. *Biomaterials* **67**, 393-407. [Crossref]
19. Jonathan M. Grasman, Michelle J. Zayas, Raymond L. Page, George D. Pins. 2015. Biomimetic scaffolds for regeneration of volumetric muscle loss in skeletal muscle injuries. *Acta Biomaterialia* **25**, 2-15. [Crossref]
20. Neal Devin, Sakar Mahmut Selman, Bashir Rashid, Chan Vincent, Asada Haruhiko Harry. 2015. Mechanical Characterization and Shape Optimization of Fascicle-Like 3D Skeletal Muscle Tissues Contracted with Electrical and Optical Stimuli. *Tissue Engineering Part A* **21**:11-12, 1848-1858. [Abstract] [Full Text HTML] [Full Text PDF] [Full Text PDF with Links] [Supplemental Material]

21. K.W. VanDusen, L.M. Larkin. Muscle–tendon interface 409-429. [Crossref]